Metabolic Engineering 64 (2021) 167–179

Contents lists available at ScienceDirect

Metabolic Engineering

journal homepage: www.elsevier.com/locate/meteng

Characterization of aromatic acid/proton symporters in *Pseudomonas putida* KT2440 toward efficient microbial conversion of lignin-related aromatics

Ayumu Wada [a], Érica T. Prates [b,d], Ryo Hirano [a], Allison Z. Werner [c,d], Naofumi Kamimura [a], Daniel A. Jacobson [b,d], Gregg T. Beckham [c,d], Eiji Masai [a,*]

[a] Department of Bioengineering, Nagaoka University of Technology, Nagaoka, Niigata, Japan
[b] Biosciences Division, Oak Ridge National Laboratory, Oak Ridge, TN, USA
[c] Renewable Resources and Enabling Sciences Center, National Renewable Energy Laboratory, Golden, CO, 80401, USA
[d] Center for Bioenergy Innovation, Oak Ridge National Laboratory, Oak Ridge, TN, USA

ARTICLE INFO

Keywords:
Pseudomonas putida
Lignin
Aromatic acids
Major facilitator superfamily
Aromatic acid/H^+ symporter

ABSTRACT

Pseudomonas putida KT2440 (hereafter KT2440) is a well-studied platform bacterium for the production of industrially valuable chemicals from heterogeneous mixtures of aromatic compounds obtained from lignin depolymerization. KT2440 can grow on lignin-related monomers, such as ferulate (FA), 4-coumarate (4CA), vanillate (VA), 4-hydroxybenzoate (4HBA), and protocatechuate (PCA). Genes associated with their catabolism are known, but knowledge about the uptake systems remains limited. In this work, we studied the KT2440 transporters of lignin-related monomers and their substrate selectivity. Based on the inhibition by protonophores, we focused on five genes encoding aromatic acid/H^+ symporter family transporters categorized into major facilitator superfamily that uses the proton motive force. The mutants of *PP_1376* (*pcaK*) and *PP_3349* (*hcnK*) exhibited significantly reduced growth on PCA/4HBA and FA/4CA, respectively, while no change was observed on VA for any of the five gene mutants. At pH 9.0, the conversion of these compounds by *hcnK* mutant (FA/4CA) and *vanK* mutant (VA) was dramatically reduced, revealing that these transporters are crucial for the uptake of the anionic substrates at high pH. Uptake assays using ^{14}C-labeled substrates in *Escherichia coli* and biosensor-based assays confirmed that PcaK, HcnK, and VanK have ability to take up PCA, FA/4CA, and VA/PCA, respectively. Additionally, analyses of the predicted protein structures suggest that the size and hydropathic properties of the substrate-binding sites of these transporters determine their substrate preferences. Overall, this study reveals that at physiological pH, PcaK and HcnK have a major role in the uptake of PCA/4HBA and FA/4CA, respectively, and VanK is a VA/PCA transporter. This information can contribute to the engineering of strains for the efficient conversion of lignin-related monomers to value-added chemicals.

1. Introduction

Lignin is a major component of the plant cell wall and the largest source of renewable aromatic compounds in nature. Although lignin is still underutilized industrially, there is a strong drive for the use of lignin as a renewable resource (Ragauskas et al., 2014). In recent years, the production of useful chemicals, such as *cis,cis*-muconate, 2-pyrone-4, 6-decarboxylate, and polyhydroxyalkanoates from lignin has been reported as a "biological funneling" process, which combines chemo-catalytic depolymerization of lignin with the bacterial metabolic ability to catabolize heterogeneous lignin-related aromatic compounds (Becker and Wittmann, 2019; Beckham et al., 2016; Johnson et al., 2019; Linger et al., 2014; Suzuki et al., 2020).

Pseudomonas putida KT2440 (hereafter KT2440) is a widely utilized microbial chassis for biological funneling due to its metabolic ability for a wide range of substrates, high growth rate, and high environmental stress resistance (Loeschcke and Thies, 2015; Nikel et al., 2016; Poblete-Castro et al., 2012; Weimer et al., 2020). KT2440 is well characterized and has a metabolic system for some of the primary lignin-related monomers, such as ferulate (FA), 4-coumarate (4CA, also referred to as *p*-coumarate), vanillate (VA), 4-hydroxybenzoate (4HBA), and protocatechuate (PCA) (Jiménez et al., 2002). Therefore, KT2440 has been used as a platform microorganism for bioproduction of industrially useful substances from lignin-related monomers (Johnson et al., 2019;

* Corresponding author.
E-mail address: emasai@vos.nagaokaut.ac.jp (E. Masai).

https://doi.org/10.1016/j.ymben.2021.01.013
Received 15 October 2020; Received in revised form 10 December 2020; Accepted 30 January 2021
Available online 4 February 2021
1096-7176/© 2021 International Metabolic Engineering Society. Published by Elsevier Inc. All rights reserved.

Salvachúa et al., 2018, 2020; Sonoki et al., 2017). To date, a great deal of knowledge has been accumulated regarding the genes, enzymes, and the regulation of catabolic pathways involved in the bacterial degradation of FA, 4CA, VA, 4HBA, and PCA (Bugg et al., 2011; Jiménez et al., 2002; Johnson et al., 2017; Kamimura et al., 2017; Masai et al., 2007; Ravi et al., 2017). However, knowledge regarding the uptake of lignin-related monomers into cells is considerably limited. Elucidation of aromatic uptake system will contribute to engineering strains capable of efficiently converting lignin-related monomers into value-added chemicals.

Phenolic carboxylic acids, such as lignin-related monomers, have been predicted with molecular dynamics simulations to minimally passively diffuse across cell membranes at physiological pH due to ionization of the carboxyl group (Vermaas et al., 2019). Therefore, it is considered likely that bacteria utilize active transporters to efficiently take up FA, 4CA, VA, 4HBA, and PCA. To date, transporters involved in, or presumed to be involved in, the inner membrane transport of lignin-related monomers in bacteria were found to belong to several classes, including: major facilitator superfamily (MFS) transporter (Chaudhry et al., 2007; D'Arrigo et al., 2019; D'Argenio et al., 1999; Harwood et al., 1994; Hopf et al., 2019; Kallscheuer et al., 2016; Kamimura et al., 2010; Mori et al., 2018a; Nichols and Harwood, 1997; Nogales et al., 2011; Otani et al., 2014; Pernstich et al., 2014), ATP-binding cassette (ABC) transporter (Chen et al., 2017; MacLean et al., 2011; Michalska et al., 2012; Salmon et al., 2013), tripartite ATP-independent periplasmic transporter (TRAP-T) (Frank et al., 2018; Salmon et al., 2013), and divalent anion/Na^+ symporter (DASS) (Reveron et al., 2017). Porins and channels are involved in the transport of lignin-related monomers across the outer membrane, like the substrate-specific channel OpdK in *Pseudomonas aeruginosa* (Biswas et al., 2008). Further, the putative porin *PP_3350* was recently shown to be an important genetic target for increasing strain tolerance towards high concentrations of 4CA in KT2440 (Mohamed et al., 2020). Additionally, it was recently reported that an active transport system mediated by a TonB-dependent receptor utilizing the proton motive force is involved in the outer membrane transport of a biphenyl-type lignin-related aromatic compound in *Sphingobium* sp. SYK-6 (Fujita et al., 2019).

The MFS transporters [2.A.1. in the Transporter Classification Database (Saier et al., 2016)] (Pao et al., 1998; Reddy et al., 2012) involved in the uptake of lignin-related monomers reported so far are categorized into the aromatic acid/H^+ symporter (AAHS) family (2.A.1.15) and metabolite/H^+ symporter (MHS) family (2.A.1.6). Pioneering work studying the AAHS family transporter PcaK from *P. putida* PRS2000 using radio-labeled substrates revealed that PcaK uptakes PCA and 4HBA coupled with proton uptake (Harwood et al., 1994; Nichols and Harwood, 1997). Disruption of *pcaK* in PRS2000 significantly affected the growth of this strain on PCA and 4HBA, thus indicating that PcaK is the primary transporter of these substrates. PcaK of *Acinetobacter baylyi* ADP1 was shown to transport VA with PCA and 4HBA by reconstitution of PcaK in proteoliposome (Pernstich et al., 2014). D'Argenio et al. reported that disruption of both *pcaK* and another AAHS family transporter gene named *vanK* in ADP1 affected the growth on PCA but not on VA (D'Argenio et al., 1999). In Gram-positive bacteria, PcaK and VanK of *Corynebacterium glutamicum* ATCC 13032 have been shown to be involved in the PCA and VA uptake, respectively, due to reduced growth of *pcaK* and *vanK* mutants on PCA and VA and their decreased conversion of PCA and VA (Chaudhry et al., 2007). However, there is a controversial result showing that *vanK* disruption did not affect the growth of ATCC 13032 on VA (Merkens et al., 2005). Thus, the involvement of the genes dubbed *vanK* is not yet apparent. In KT2440, *vanK* (*PP_3740*) is suggested to be involved in the uptake of FA based on the observation that the expression of *vanK* increased ca. 271-fold when cultured with FA, and the growth of a *vanK* mutant on FA was significantly reduced (D'Arrigo et al., 2019). On the other hand, there are three examples suggesting the involvement of MHS family transporters in the uptake of lignin-related aromatic compounds (D'Arrigo et al., 2019; Kallscheuer et al., 2016; Otani et al., 2014).

In this study, we investigated the role of five AAHS family transporter genes present in the KT2440 genome (*PP_1376*, *PP_3165*, *PP_3349*, *PP_3658*, and *PP_3740*) in the uptake system of the lignin-related monomers. We identified several genes/proteins involved in the uptake of FA/4CA and VA in addition to PCA/4HBA. Moreover, the identified transporter genes were expressed in *Escherichia coli*, and the biochemical properties were characterized.

2. Materials and methods

2.1. Bacterial strains, plasmids, culture conditions, and chemicals

The strains and plasmids used in this study are listed in Supplemental Table S1, and the PCR primers are listed in Supplemental Table S2. KT2440 and derived mutants (*see §2.4*) were grown at 30 °C with shaking (160 rpm) in lysogeny broth (LB) or Wx minimal medium (Araki et al., 2020) containing succinate or lignin-related monomers in the concentration specified for each individual experiment. *E. coli* NEB 10-beta was grown in LB at 37 °C. The media for *E. coli* transformants carrying antibiotic resistance markers were supplemented with 100 mg-ampicillin/L, 25 mg-kanamycin (Km)/L, 12.5 mg-gentamycin (Gm)/L, or 50 mg-spectinomycin (Sp)/L. When necessary, the media for KT2440 and derived mutants were supplemented with 50 mg-Km/L or 12.5 mg-Gm/L. Lignin-related monomers, PCA, 4HBA, VA, FA, and 4CA, were purchased from Tokyo Chemical Ind., Co., Ltd. The radiolabeled compounds [carboxy-^{14}C]PCA (55 mCi mmol^{-1}), [carboxy-^{14}C]VA (55 mCi mmol^{-1}), and [carboxy-^{14}C]4CA (55 mCi mmol^{-1}) were purchased from American Radiolabeled Chemicals, Inc. (MO, USA).

2.2. Sequence analysis and construction of a phylogenetic tree

Sequence analysis was performed using the MacVector program (MacVector, Inc., NC, USA). Sequence similarity searches were performed using the BLASTP program at the NCBI server and PSI-BLAST at the Transporter Classification Database (Saier et al., 2016). Pairwise and multiple alignments were conducted using the EMBOSS-Needle program (Madeira et al., 2019) and the Clustal Omega program (Madeira et al., 2019), respectively. For phylogenetic analysis, multiple alignments were performed by the Clustal Omega program, and then a phylogenetic tree was generated using the FigTree program (http://tree.bio.ed.ac.uk/software/figtree).

2.3. Resting cell assay

The cells of KT2440 and derived mutants were cultured in LB, harvested by centrifugation at 14,100×*g* at 4 °C for 1 min, washed twice with 3 mL of Wx medium without the metal solution (solution II) (Araki et al., 2020), and resuspended in the same medium. The cells were then inoculated in Wx medium containing 5 mM succinate with 5 mM PCA, 4HBA, VA, FA, or 4CA to an OD_{600} of 0.4, and incubated for 4 h. For the complementation analysis of KT2440 Δ*vanK* (Δ*vanK*), cells of Δ*vanK* harboring pSEVA224 or pSEVAVanK and cells of KT2440 harboring pSEVA224 were grown in Wx medium containing 1 mM isopropyl-β-D-thiogalactopyranoside (IPTG), 5 mM succinate, and 5 mM VA for 8 h. After culture, cells were harvested by centrifugation at 14,100×*g* at 4 °C for 1 min, washed twice with 50 mM Tris-HCl buffer (pH 7.5), and resuspended in the same buffer. The resultant resting cells were incubated with 1 mM PCA, 0.5 mM 4HBA, 0.5 mM VA, and 0.5 mM FA, and 0.5 mM 4CA at OD_{600} of 0.2, 0.2, 0.5, 0.5, and 0.5, respectively, and the mixtures were incubated at 30 °C with shaking at 1500 rpm in a shaker (Bioshaker M-BR-022UP, TAITEC, Saitama, Japan). For the inhibition experiments, resting cells were preincubated with carbonyl cyanide *m*-chlorophenylhydrazone (CCCP, 100 μM or 200 μM) or *N*, *N*′-dicyclohexylcarbodiimide (DCCD, 100 μM) at 30 °C for 5 min prior to adding the substrate. Since ethanol was used as a solvent for both inhibitors, ethanol was added to the control assay mixtures without

inhibitor (final concentration of 1% [v/v]). For investigation under alkaline pH conditions, 50 mM Tris-HCl buffer (pH 9.0) was used to wash the cultured cells and incubate them with the substrates. A portion of samples was collected periodically, and the reactions were stopped by centrifugation at 18,800×*g* at 4 °C for 15 min. The supernatants were diluted 10-fold in water, filtered, and analyzed by high-performance liquid chromatography (HPLC; Acquity UPLC system; Waters Corporation, MA, USA) using a TSKgel ODS-140HTP column (2.1 mm by 100 mm; Tosoh Corporation, Tokyo, Japan). All analyses were conducted at a flow rate of 0.5 mL/min, and the mobile phase was a mixture of 90% water and 10% acetonitrile containing 0.1% formic acid. The wavelength for detection and retention times of PCA, 4HBA, VA, FA, and 4CA were 259.6, 255.4, 260.3, 322.5, and 309.6 nm and 0.9, 1.3, 1.6, 3.7, and 2.9 min, respectively.

2.4. Construction of KT2440 mutants and E. coli expressing AAHS family transporter genes

The markerless deletion mutants were constructed using the pEMG/pSW-2 system (Martinez-Garcia and de Lorenzo, 2011). The upstream and downstream regions of each gene (regions flanking the gene plus part of the gene) were amplified by PCR with the total DNA of KT2440 and primer pairs listed in Supplemental Table S2. The resulting fragments were combined and cloned into pEMG using an NEBuilder HiFi DNA Assembly Cloning Kit (New England Biolabs, MA, USA). Plasmids obtained in *E. coli* were independently introduced into KT2440 cells by electroporation (pulse conditions: 200 Ω, 2.5 kV, 25 μF). The selection of mutant strains using an I-SceI endonuclease producing plasmid, pSW-2, and curing of pSW-2 were followed by the method described previously (Martinez-Garcia and de Lorenzo, 2011). Disruptions of each gene were examined by colony PCR using the primer pair shown in Supplemental Table S2, respectively.

The regions containing *pcaK*, *vanK*, or *hcnK* were amplified by PCR and then cloned into the *Bam*HI site of pET-16b using an NEBuilder HiFi DNA Assembly Cloning Kit to generate pETPcaK, pETVanK, and pETHcnK, respectively (Supplemental Table S1). Nucleotide sequences of amplified regions of each plasmid were confirmed by Eurofins Genomics. *E. coli* C43 (DE3) cells were transformed by the resulting plasmids.

2.5. Growth measurement

The cells of KT2440, derived mutants, and complemented strains were grown in LB for 24 h, harvested by centrifugation at 14,100×*g* at 4 °C for 1 min, washed twice with Wx medium without the metal solution, and resuspended in 1 mL of Wx medium. The cells were then inoculated in Wx medium containing 2, 5, and 20 mM PCA, 4HBA, VA, FA, or 4CA to an OD_{600} of 0.2. A portion of samples was collected periodically, and cell growth was monitored using a Gene Quant 100 Spectrophotometer (GE Healthcare, Buckinghamshire, UK). For the complementation analysis, cells of KT2440 Δ*pcaK* (Δ*pcaK*) harboring pSEVAPcaK, Δ*pcaK* harboring pSEVA224, KT2440 Δ*hcnK* (Δ*hcnK*) harboring pSEVAHcnK, Δ*hcnK* harboring pSEVA224, and KT2440 harboring pSEVA224 were grown in Wx medium containing 1 mM IPTG in addition to 5 mM PCA, VA, or FA.

2.6. Uptake assay using radiolabeled substrates

E. coli C43 (DE3) cells harboring pETPcaK, pETVanK, or pETHcnK were grown in LB at 30 °C, and gene expression was induced by addition of 1 mM IPTG at OD_{600} reached 0.5. After 4 h incubation, cells were washed twice with 50 mM Tris-HCl buffer (pH 7.5) and resuspended in the same buffer. Cell suspensions (OD_{600} = 2.4) were incubated with 12 mM glucose (total volume, 125 μL) at 30 °C for energy generation before mixing with substrates. After 5 min of incubation, uptake was initiated by the addition of 20 μM [^{14}C]PCA, 20 μM [^{14}C]VA, and 10 μM [^{14}C]4CA (25 μL) to an OD_{600} of 2.0 in a total volume of 150 μL. A portion of samples was collected from the reaction mixture at 15, 30, 45, and 60 s (the 15 s intervals were required for correct data acquisition), and immediately vacuum filtrated through nitrocellulose membranes (0.45 μm pore size; Advantec Co., Ltd., Tokyo, Japan). After the filters were washed twice with 3 mL of 50 mM Tris-HCl buffer (pH 7.5), the cell-adhered filters were dissolved in scintillation cocktail and accumulated radiolabeled substrates inside the cells were measured by liquid scintillation counting (AccuFLEX LSC-7400; Hitachi Aloca Medical, Ltd., Tokyo, Japan). Uptake rates were calculated from radioactivity from [^{14}C]PCA, [^{14}C]VA, or [^{14}C]4CA incorporated into cells 15 s after the initiation of reaction. The uptake activity was expressed as nanomoles of substrate per min per milligram of protein. To determine the amount of total protein contained in the cells used for the uptake assay, the protein concentration was determined using a DC protein assay kit (Bio-Rad Laboratories, Inc., CA, USA). For the inhibition experiments, cells were preincubated with 100 μM CCCP or 1% (v/v) ethanol in addition to 12 mM glucose. To determine the effects of lignin-related aromatic acids on PCA, VA, and 4CA uptake, cells were preincubated with 200 or 400 μM PCA, 4HBA, VA, syringate, benzoate, 3-hydroxybenzoate, gallate, FA, or 4CA in addition to 12 mM glucose. For determination of kinetic parameters, uptake rates were determined using 1, 2, 5, 10, 20, and 50 μM [^{14}C]PCA, [^{14}C]VA, and [^{14}C]4CA, and fitted to the Michaelis-Menten equation using GraphPad Prism software (version 8.0; GraphPad Software, Inc., La Jolla, CA, USA). For the measurement of kinetic parameters, uptake activities were calculated by subtracting the uptake activity of *E. coli* C43 (DE3) cells harboring pET-16b from that of *E. coli* C43 (DE3) cells harboring pETPcaK, pETVanK, or pETHcnK.

2.7. Uptake assay using a bacterial sensor for FA and 4CA

The uptake of FA and 4CA was examined using pSEVA421-B11 (RK2 *ori*) containing a *padC* promoter region-YFP gene cassette and *padR*, encoding repressor of the *padC* promoter (Siedler et al., 2017). The fragment containing *lacI*^{q}-P$_{trc}$-*hcnK* of pSEVAHcnK (RK2 *ori*) was introduced into pSEVA231 (pBBR1 *ori*) to generate pSEVAHcnK2. Cells of *E. coli* XL2-Blue harboring pSEVA421-B11 and pSEVA231 or pSEVAHcnK2 were grown in LB at 30 °C, and expression of *hcnK* was induced by the addition of 1 mM IPTG when OD_{600} reached 0.5. After 4 h incubation, cells were washed twice with Wx medium without the metal solution and resuspended in the same medium. The resulting cells were inoculated into a 96-well microtiter plate filled with 200 μl of Wx medium containing 20 μM FA or 4CA in addition to 1 mM IPTG and 5 mM glucose to an OD_{600} of 0.2 and grown with shaking (1000 rpm) at 30 °C in a plate shaker (Bioshaker M-BR-022UP, TAITEC). After 18 h, fluorescence (excitation, 485 nm; emission, 528 nm) and OD_{600} were measured using a Synergy LX microplate reader (BioTek, VT, USA). The uptake activities were calculated as fluorescence intensity per OD_{600} of the cells.

2.8. Protein structure analysis

Close homologs with solved structures are not available to enable homology modeling of the putative MFS transporters studied here. Therefore, *de novo* modeling of PcaK, HcnK, VanK, and PP_3658 was performed guided by predicted evolutionary couplings between sites using the EVcoupling framework (Hopf et al., 2019), which has shown good results in comparative studies of modeling techniques for membrane proteins (Hopf et al., 2012; Koehler Leman et al., 2015). Predicted intrinsically disordered termini were not included. The local quality of the models was estimated using the combined statistical potentials of QMEANBrane (Studer et al., 2014). Transmembrane regions, which are the main focus of this study, exhibited good quality estimates for the three models. ClustalW (Larkin et al., 2007) was used for primary sequence alignment. Visual analysis and the design of figures were performed using VMD 1.93 (Humphrey et al., 1996).

2.9. Statistical analysis

Statistical tests were performed using GraphPad Prism 8 (GraphPad software). One-way ANOVA with Dunnett's test and Student's *t*-test were used for multiple and pairwise comparisons, respectively. $P < 0.05$ was considered statistically significant.

3. Results

3.1. Determination of energy requirements for lignin-related monomer uptake

To gain insight into the energy required for the uptake of lignin-related monomers that exhibit a carboxylate group, including PCA, 4HBA, VA, FA, and 4CA, we examined the capability of *P. putida* KT2440 cells to convert these substrates in the presence of the protonophore CCCP or the inhibitor of ATP synthase DCCD. KT2440 cells grown in Wx medium containing 5 mM succinate with 5 mM PCA, 4HBA, VA, FA, or 4CA were incubated with corresponding substrates (0.5 or 1.0 mM) in the presence and absence of CCCP (100 or 200 μM) or DCCD (100 μM), and substrate conversions were monitored (Fig. 1 and Supplemental Table S3). While almost no inhibition was observed in the presence of DCCD, conversion rates were significantly ($P < 0.05$, one-way ANOVA with Dunnett's multiple comparisons post-test) reduced in the presence of CCCP. These results suggest that transporters, which require the proton motive force, are involved in the uptake of these monomers.

3.2. Characterization of disruption mutants of aromatic acid/H^+ symporter (AAHS) family transporter genes

In the *P. putida* KT2440 genome, we identified 70 genes encoding putative MFS transporters, which require the proton motive force. Phylogenetic analysis revealed that these MFS transporters include five AAHS family transporter genes and 14 metabolite/H^+ symporter (MHS) family transporter genes (Supplemental Fig. S1). Based on the fact that many reports demonstrated the involvement of AAHS family transporters in the uptake of aromatic acids (Chaudhry et al., 2007; Collier et al., 1997; D'Arrigo et al., 2019; Mori et al., 2018a; Nichols and Harwood, 1997; Nogales et al., 2011; Pernstich et al., 2014; Xu et al., 2013; Xu et al., 2012), we focused here on the AAHS family transporter genes (*PP_1376*, *PP_3165*, *PP_3349*, *PP_3658*, and *PP_3740*). *PP_1376* (annotated as *pcaK*), which shows 97.5% amino acid sequence identity with PCA/4HBA transporter PcaK of *P. putida* PRS 2000, is located in the *pca* gene cluster. *PP_1376* (*pcaK*) has recently been predicted to transport PCA but not 4HBA based on the analysis of randomly barcoded transposon mutants (Incha et al., 2020). *PP_3165* (annotated as *benK*) located in the benzoate catabolic gene cluster shows 45.1% amino acid sequence identity with benzoate transporter (BenK) of *A. baylyi* ADP1. *PP_3165* (*benK*) conferred the ability of yeast cells to uptake benzoate (Nishikawa et al., 2008). *PP_3349* (annotated as *mhpT*) located approximately 7.4-kb downstream of the FA catabolic genes shows 54.9% amino acid sequence identity with 3-(3-hydroxyphenyl)propionate transporter MhpT of *E. coli* K-12 (Xu et al., 2013). *PP_3658* is located just upstream of the *p*-nitrobenzoate reductase gene (*nfnB*) and shows 37.1% amino acid sequence identity with BenK of *A. baylyi* ADP1. *PP_3740* (annotated as *vanK*) is localized near the vanillate *O*-demethylase genes (*vanAB*)

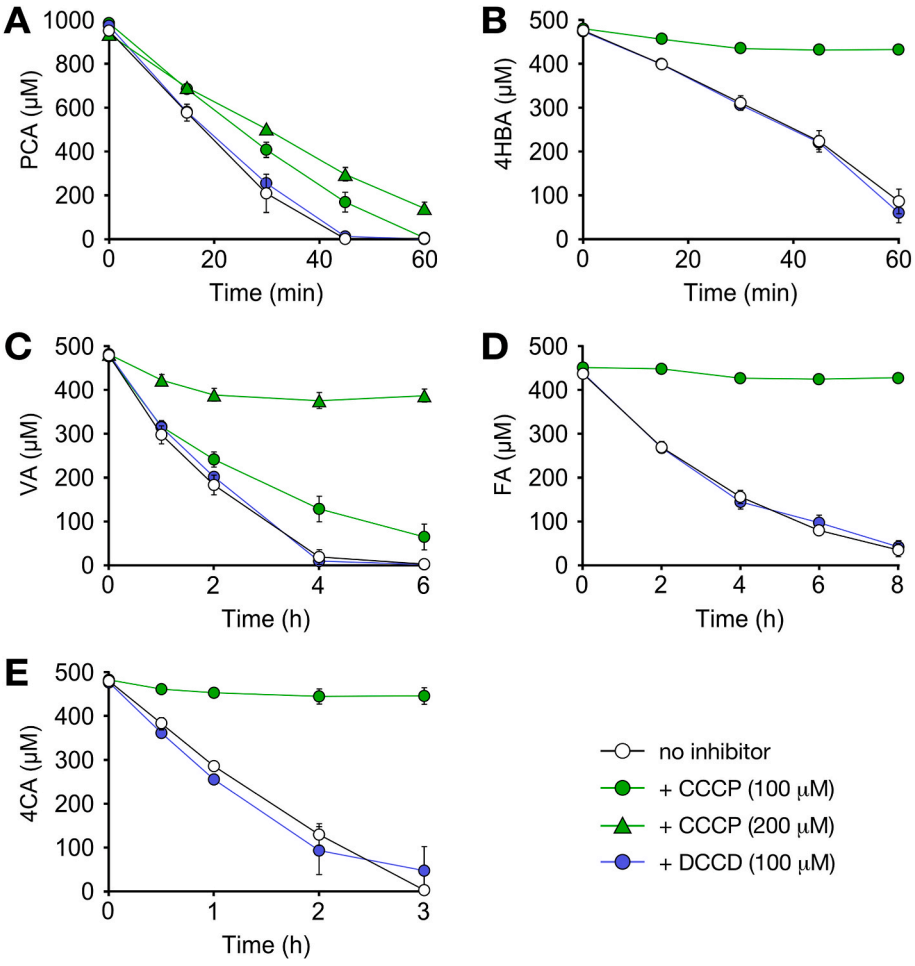

Fig. 1. Conversion of lignin-related monomers by KT2440 in the presence of CCCP or DCCD. KT2440 cells were grown in Wx medium containing 5 mM succinate with 5 mM PCA, 4HBA, VA, FA, or 4CA. The resulting cells were preincubated for 5 min with 100 μM CCCP (green circles), 200 μM CCCP (green triangles), 100 μM DCCD (blue circles), or 1% ethanol ([v/v], a solvent used to prepare inhibitor solutions; white circles), and then the cells were incubated with the same substrate used during cultivation; 1 mM PCA (**A**; OD_{600} = 0.2), 0.5 mM 4HBA (**B**; OD_{600} = 0.2), 0.5 mM VA (**C**; OD_{600} = 0.5), 0.5 mM FA (**D**; OD_{600} = 0.5), and 0.5 mM 4CA (**E**; OD_{600} = 0.5). Portions of the reaction mixtures were collected, and the amounts of substrates was measured by HPLC. Each value is the average ± the standard deviation of three independent experiments. (For interpretation of the references to colour in this figure legend, the reader is referred to the Web version of this article.)

and shows 53.8% amino acid sequence identity with PCA/4HBA transporter (VanK) of *A. baylyi* ADP1. *PP_3740* (*vanK*) is predicted to be involved in the uptake of FA due to the retarded growth of a *vanK* mutant on FA (D'Arrigo et al., 2019).

To examine the involvement of the five AAHS family transporter genes in the uptake of the lignin-related monomers, we knocked out each gene from the *P. putida* genome individually, generating strains Δ*pcaK*, Δ*benK*, Δ*mhpT*, Δ*PP_3658,* and Δ*vanK* (Supplemental Fig. S2A–E). The capacities of these mutant cells to grow on the lignin-related monomers were examined by incubating the mutant cells in Wx minimal medium (pH 7.1) containing 5 mM PCA, 4HBA, VA, FA, or 4CA as a sole carbon and energy source (Fig. 2). Among the mutants, Δ*pcaK* cells almost lost the capacity to grow on PCA and exhibited a considerably retarded growth on 4HBA (Fig. 2A and B; Supplemental Table S4). Moreover, Δ*mhpT* cells showed significant and moderate growth retardations on FA and 4CA, respectively (Fig. 2D and E; Supplemental Table S4). The introduction of a *pcaK*- and an *mhpT*-carrying plasmid into cells of Δ*pcaK* and Δ*mhpT*, respectively, restored the growth of these cells on PCA/4HBA and FA (Supplemental Fig. S3). These results indicate that the growth reductions observed in Δ*pcaK* on PCA/4HBA and Δ*mhpT* on FA/4CA were caused by disruption of *pcaK* and *mhpT*, respectively. Based on the predicted function of *PP_3349* (*mhpT*), we reannotated *PP_3349* from *mhpT* (*m*-hydroxyphenylpropionate transporter gene) to *hcnK* (*p*-hydroxycinnamate transporter gene). In contrast, the disruption of these genes did not significantly affect the growth of KT2440 cells on VA (Fig. 2C and Supplemental Table S4).

The mutant cells of the five AAHS family transporter genes grown in Wx minimal medium containing 5 mM succinate with 5 mM PCA, 4HBA, VA, FA, or 4CA were incubated with each lignin-related monomer (0.5 or 1.0 mM) in 50 mM Tris-HCl buffer (pH 7.5), and conversions of substrates were monitored (Fig. 3). The amounts of PCA and 4HBA converted by Δ*pcaK* cells decreased to ca. 15% and 5% of the quantities transformed by wild-type cells at 30 min, the time in which conversions by wild-type and mutant cells proceed in an almost linear fashion (Fig. 3A and B; Supplemental Table S5). The amounts of FA and 4CA converted by Δ*hcnK* cells reduced to ca. 39% and 24% of those transformed by wild-type KT2440 at 2 and 3 h, respectively (Fig. 3D and E; Supplemental Table S5). These results are in agreement with the reduced growth of Δ*pcaK* and Δ*hcnK* cells, suggesting that *pcaK* and *hcnK* are involved in the uptake of PCA/4HBA and FA/4CA, respectively. Δ*vanK* showed slightly decreased conversions of VA, FA, and 4CA (ca. 77% at 1 h, 73% at 2 h, and 88% at 3 h of wild-type conversion, respectively; Fig. 3C–E; Supplemental Table S5). The introduction of a *vanK*-carrying plasmid (pSEVAVanK) into Δ*vanK* cells increased the conversion rate of VA (Supplemental Fig. S4), suggesting that a decrease in VA conversion was caused by *vanK* disruption.

Since Δ*pcaK* and Δ*vanK* cells showed slight decreases in the conversion of VA and FA, respectively (Fig. 3C and D; Supplemental Table S5), we created Δ*vanK pcaK* and Δ*hcnK vanK* (Supplemental

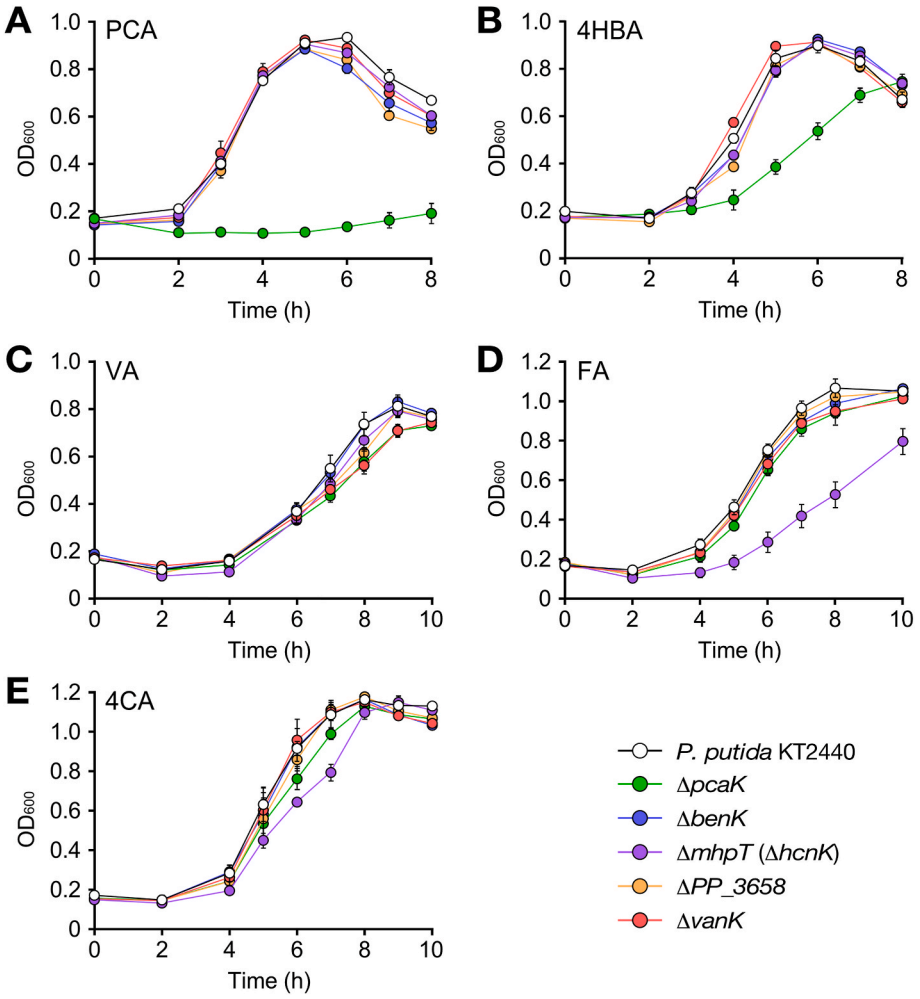

Fig. 2. Growth of mutants of putative AAHS family transporter genes on lignin-related monomers. Cells of wild-type KT2440, Δ*pcaK*, Δ*benK*, Δ*mhpT* (Δ*hcnK*), Δ*PP_3658*, and Δ*vanK* were cultured in Wx medium containing 5 mM PCA (**A**), 4HBA (**B**), VA (**C**), FA (**D**), and 4CA (**E**). Cell growth was monitored by measuring the OD_{600}. Each value is the average ± the standard deviation of three independent experiments.

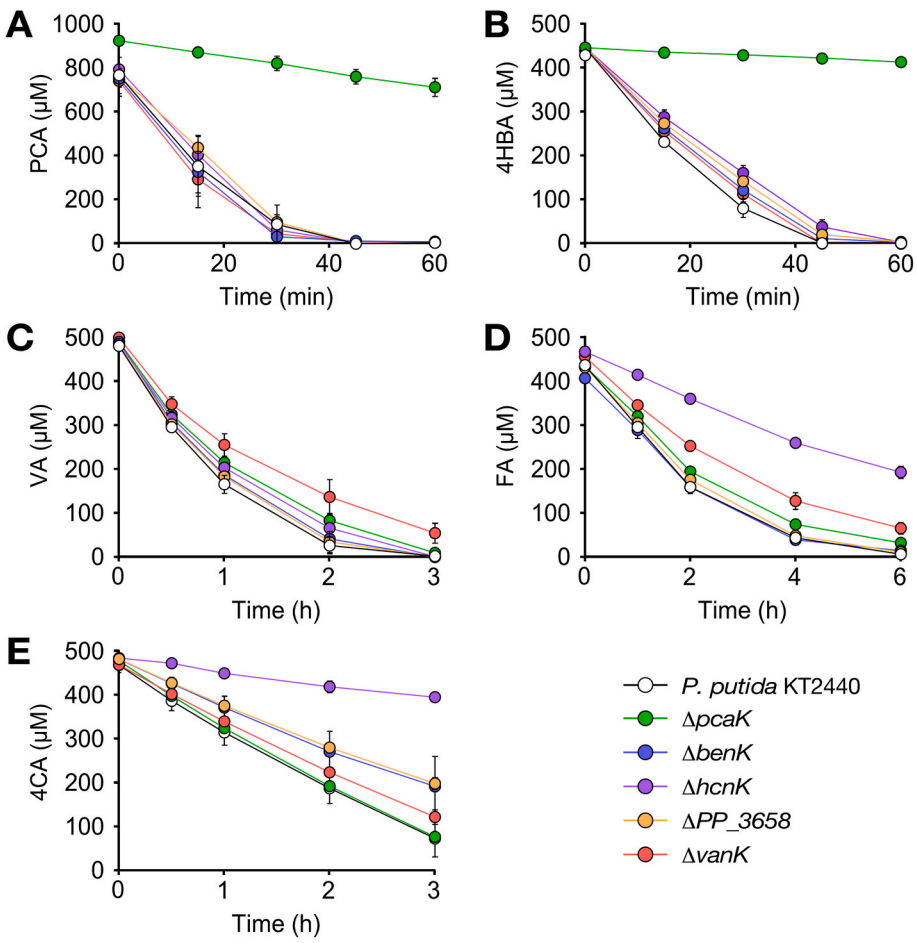

Fig. 3. Conversion of lignin-related monomers by mutants of putative AAHS family transporter genes. Cells of wild-type KT2440, Δ*pcaK*, Δ*benK*, Δ*hcnK*, Δ*PP_3658*, and Δ*vanK* were grown in Wx medium containing 5 mM succinate with 5 mM PCA, 4HBA, VA, FA, or 4CA. The resulting cells were incubated with the corresponding substrates; 1 mM PCA (**A**; OD_{600} = 0.2), 0.5 mM 4HBA (**B**; OD_{600} = 0.2), 0.5 mM VA (**C**; OD_{600} = 0.5), 0.5 mM FA (**D**; OD_{600} = 0.5), and 0.5 mM 4CA (**E**; OD_{600} = 0.5) in 50 mM Tris-HCl buffer (pH 7.5). Portions of the reaction mixtures were collected, and the amounts of substrates were measured by HPLC. Each value is the average ± the standard deviation of three independent experiments.

Fig. S2F and G) and examined the substrate conversion capacity of these cells grown with VA or FA to convert the substrates, respectively. The amount of VA converted by Δ*vanK pcaK* cells was reduced as compared to Δ*vanK* cells (ca. 59% of the amount transformed by wild-type cells at 1 h, Supplemental Fig. S5A). The amount of FA converted by Δ*hcnK vanK* cells also further decreased (ca. 21% of the amount transformed by wild-type cells at 2 h, Supplemental Fig. S5B). These results suggest that *pcaK* and *vanK* partially participate in the uptake of VA and FA, respectively.

3.3. Growth of ΔpcaK, ΔvanK, and ΔhcnK on different concentrations of lignin-related monomers

Although the capability of Δ*pcaK* and Δ*hcnK* cells to convert 0.5 mM 4HBA and 4CA, respectively, was significantly reduced (Fig. 3 and Supplemental Table S5), the decrease in their growth on 5 mM of the corresponding substrates was less significant (Fig. 2). These results may imply that the use of higher concentrations of substrate for growth measurements resulted in the uptake by other transporters that show low affinity toward the substrates. Therefore, we evaluated the growth of Δ*pcaK*, Δ*vanK*, and Δ*hcnK* in Wx medium (pH 7.1) containing 2, 5, and 20 mM lignin-related monomers as a carbon and energy source (Fig. 4). As for the growth of Δ*pcaK* on PCA, loss of growth was observed at all concentrations (Fig. 4A). At 2 mM and 5 mM 4HBA, Δ*pcaK* cells showed an extended lag phase and slow growth rate compared to the wild-type cells; however, the growth at 20 mM was almost the same as that of the wild-type cells (Fig. 4B). In contrast, the growth of Δ*vanK* cells on VA showed almost no difference from the wild-type cells at all concentrations (Fig. 4C). The growth of Δ*hcnK* cells on FA was significantly reduced at 2 and 5 mM, but there was little difference at 20 mM from the wild-type growth (Fig. 4D). The growth of Δ*hcnK* cells on 4CA was considerably reduced at 2 mM but was equivalent to the wild-type cells at 5 and 20 mM (Fig. 4E). Since Δ*pcaK* cells did not grow on PCA at all concentrations, *pcaK* appears to be essential for PCA uptake. Regarding 4HBA, FA, and 4CA, as their concentrations increased, the growth profiles of Δ*pcaK* and Δ*hcnK* cells became equivalent to those of wild-type cells. Hence, the influence of gene disruption was not observed for the growth of the mutants on 20 mM 4HBA, FA, and 4CA, probably due to the uptake of substrates by unknown transporters exhibiting lower affinity for these compounds. On the other hand, a considerable part of VA appears to be taken up by transporters other than VanK.

3.4. Conversion of lignin-related monomers by ΔpcaK, ΔvanK, and ΔhcnK under alkaline pH condition

Under an alkaline pH condition (50 mM Tris-HCl [pH 9.0]) that increases the abundance of ionized substrates (the fractions of carboxylate of PCA [pK_{a1}, 4.62; pK_{a2}, 8.90; pK_{a3}, 10.73], 4HBA [pK_{a1}, 4.66; pK_{a2}, 9.19], VA [pK_{a1}, 4.65; pK_{a2}, 9.21], FA [pK_{a1}, 4.66; pK_{a2}, 9.09], and 4CA [pK_{a1}, 4.92; pK_{a2}, 9.28] are more than 99.99%) (Beltrán et al., 2003), cells of Δ*pcaK*, Δ*vanK*, and Δ*hcnK* grown in Wx-5 mM succinate with 5 mM PCA/4HBA, VA, or FA/4CA, respectively, were incubated with 0.5 mM of corresponding substrates. The conversion of the substrates was examined and compared to that under physiological pH condition (pH 7.5; the fractions of carboxylate of PCA, 4HBA, VA, FA, and 4CA are 99.87%, 99.86%, 99.86%, 99.86%, and 99.74%). PCA conversion by Δ*pcaK* cells at pH 7.5 after 30 min reduced to ca. 20% of that by the wild-type cells, and this reduction was practically equal to that measured at pH 9.0 (ca. 17%) (Fig. 5A). 4HBA conversion by Δ*pcaK* cells

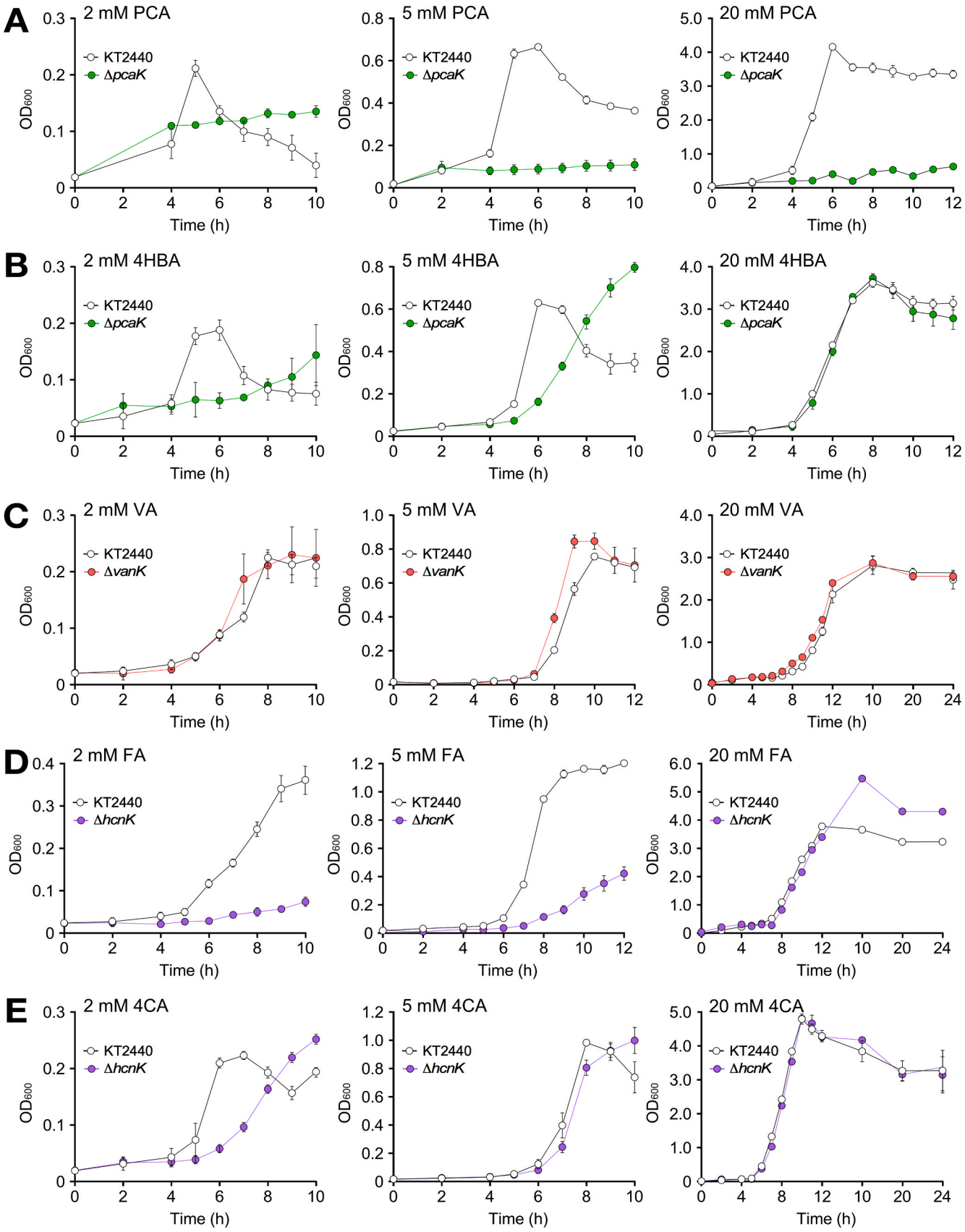

Fig. 4. Growth of Δ*pcaK*, Δ*vanK*, and Δ*hcnK* on different concentrations of lignin-related monomers. (**A and B**) Cells of wild-type KT2440 and Δ*pcaK* were cultured in Wx medium containing 2, 5, and 20 mM PCA (**A**) and 4HBA (**B**). (**C**) Cells of KT2440 and Δ*vanK* were cultured in Wx medium containing 2, 5, and 20 mM VA. (**D and E**) Cells of KT2440 and Δ*hcnK* were cultured in Wx medium containing 2, 5, and 20 mM FA (**D**) and 4CA (**E**). Cell growth was monitored by measuring the OD_{600}. Each value is the average ± the standard deviation of four independent experiments.

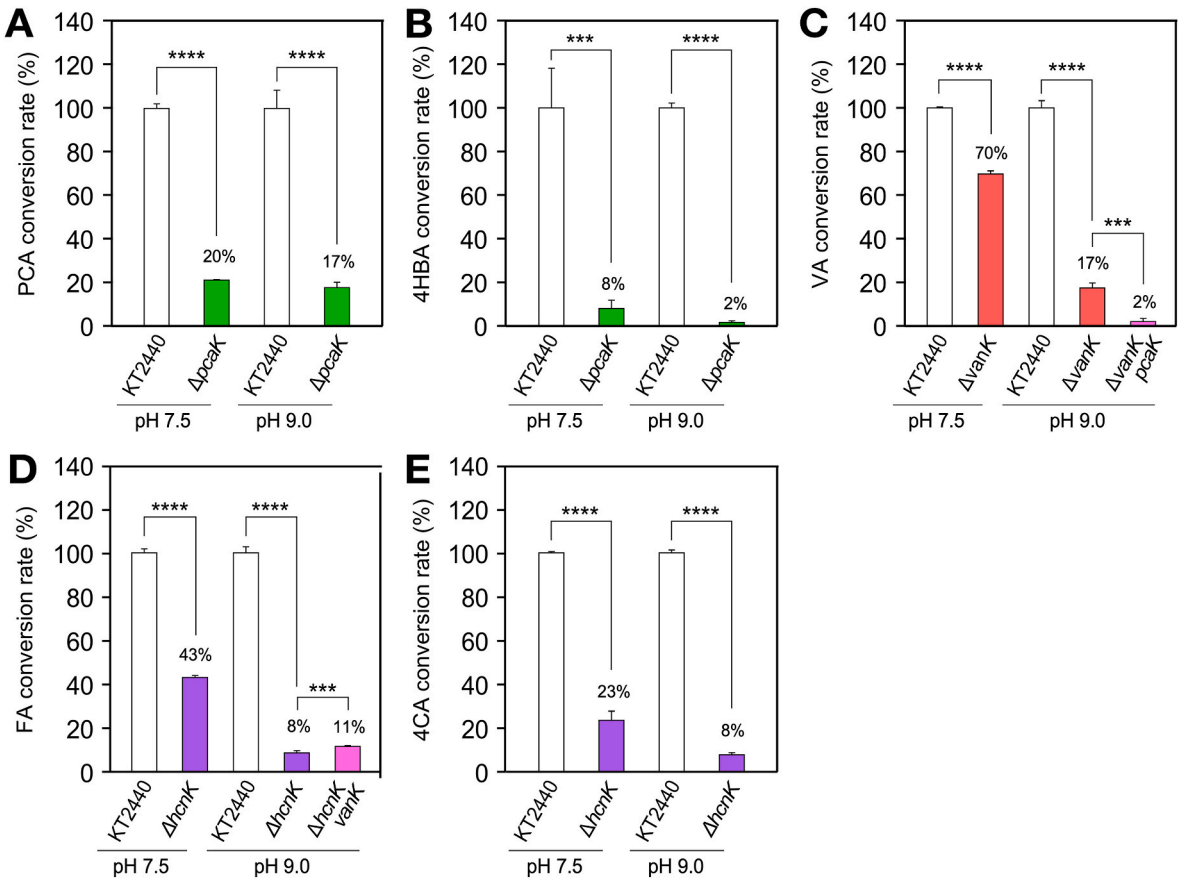

Fig. 5. Conversion of lignin-related monomers by Δ*pcaK*, Δ*vanK*, and Δ*hcnK* under alkaline pH conditions. (**A**) Cells of KT2440 and Δ*pcaK* (OD_{600} = 0.2) grown in Wx-5 mM succinate + 5 mM PCA were incubated with 1 mM PCA in 50 mM Tris-HCl buffer (pH 7.5 and 9.0) at 30 °C. (**B**) Cells of KT2440 and Δ*pcaK* (OD_{600} = 0.2) grown in Wx-5 mM succinate + 5 mM 4HBA were incubated with 0.5 mM 4HBA at pH 7.5 and 9.0. (**C**) Cells of KT2440, Δ*vanK*, and Δ*vanK pcaK* (OD_{600} = 0.5) grown in Wx-5 mM succinate + 5 mM VA were incubated with 0.5 mM VA at pH 7.5 and 9.0. (**D**) Cells of KT2440, Δ*hcnK*, and Δ*hcnK vanK* (OD_{600} = 0.5) grown in Wx-5 mM succinate + 5 mM FA were incubated with 0.5 mM FA at pH 7.5 and 9.0. (**E**) Cells of KT2440 and Δ*hcnK* (OD_{600} = 0.5) grown in Wx-5 mM succinate + 5 mM 4CA were incubated with 0.5 mM 4CA at pH 7.5 and 9.0. Portions of the reaction mixtures were collected, and the amount of substrates was measured by HPLC. The rate of conversion of PCA, 4HBA, VA, FA, and 4CA were calculated at 30, 30, 60, 120, and 60 min, (the time in which conversions proceed in an almost linear fashion) respectively. Conversions of PCA for 30 min at pH 7.5 (573 ± 17 μM) and pH 9.0 (537 ± 49 μM), 4HBA for 30 min at pH 7.5 (208 ± 38 μM) and pH 9.0 (318 ± 16 μM), VA for 60 min at pH 7.5 (374 ± 3 μM) and pH 9.0 (337 ± 12 μM), FA for 120 min at pH 7.5 (192 ± 4 μM) and pH 9.0 (405 ± 9 μM), and 4CA for 60 min at pH 7.5 (254 ± 2 μM) and pH 9.0 (239 ± 3 μM) by KT2440 cells were set as 100% rates (control). Each value is the average ± the standard deviation of three independent experiments. Statistical differences were determined by Student's *t*-test. Asterisks indicate statistically significant difference between values linked by brackets (***, $P < 0.001$; ****, $P < 0.0001$).

at pH 7.5 after 30 min reduced to ca. 8% of that by the wild-type cells, and the conversion at pH 9.0 reduced to ca. 2% (Fig. 5B). VA conversion by Δ*vanK* cells was only reduced to ca. 70% of that by the wild-type cells at pH 7.5 after 1 h but was significantly reduced to ca. 17% at pH 9.0 (Fig. 5C). Further, VA conversion by Δ*vanK pcaK* cells at pH 9.0 was reduced to ca. 2% of that by the wild-type cells. FA conversion by Δ*hcnK* cells at pH 7.5 after 2 h reduced to ca. 43% of that by the wild-type cells, and at pH 9.0, it was significantly reduced to ca. 8% (Fig. 5D). The decrease in FA conversion by Δ*hcnK vanK* cells at pH 9.0 was approximately equal to that by Δ*hcnK* cells. 4CA conversion by Δ*hcnK* cells at pH 7.5 after 1 h reduced to ca. 23% of that by wild-type cells, and at pH 9.0, it was significantly reduced to ca. 8% of that by wild-type cells (Fig. 5E).

3.5. Properties of PcaK, VanK, and HcnK

Properties of PcaK. Cells of *E. coli* C43 (DE3) harboring a *pcaK*-expressing plasmid (pETPcaK) (OD_{600} of 2.0) were incubated with 20 μM [^{14}C]PCA, 20 μM [^{14}C]VA, or 10 μM [^{14}C]4CA at pH 7.5, and the time course of uptake of each substrate by *E. coli* (pETPcaK) cells was monitored. These cells showed PCA uptake activity (10.1 ± 0.9 nmol min^{-1} mg^{-1}; calculated by subtracting the vector control uptake amount from the uptake amount of *E. coli* [pETPcaK] after 15 s) and also slightly exhibited VA uptake activity (0.46 ± 0.04 nmol min^{-1} mg^{-1}) (Fig. 6A and B). However, the uptake of 4CA was not observed (Fig. 6C). K_m and V_{max} of PCA uptake by *E. coli* (pETPcaK) cells were estimated to be 8.1 ± 1.5 μM and 17.4 ± 1.1 nmol min^{-1} mg^{-1}, respectively (Supplemental Fig. S6). The PCA uptake rate by *E. coli* (pETPcaK) cells decreased to ca. 3.6% in the presence of 100 μM CCCP compared to the control without CCCP, indicating that PcaK required the proton motive force (Supplemental Fig. S7).

To anticipate the substrates recognized by PcaK, we measured the [^{14}C]PCA (20 μM) uptake rates by *E. coli* (pETPcaK) cells at pH 7.5 in the presence of 20-fold concentration (400 μM) of unlabeled competitor substrates. In the presence of competitors other than syringate, FA, and 4CA, the PCA uptake rates reduced to 12–78% of that in the absence of competitors (Supplemental Fig. S8). In particular, the PCA uptake rates in the presence of PCA and 4HBA reduced to ca. 12% and 19% of that in the absence of the competitors, respectively. These results support that PcaK is involved in 4HBA uptake. By contrast, in the presence of VA, where PcaK showed weak uptake (ca. 5% of activity for PCA uptake), the PCA uptake rate was only reduced to ca. 78%.

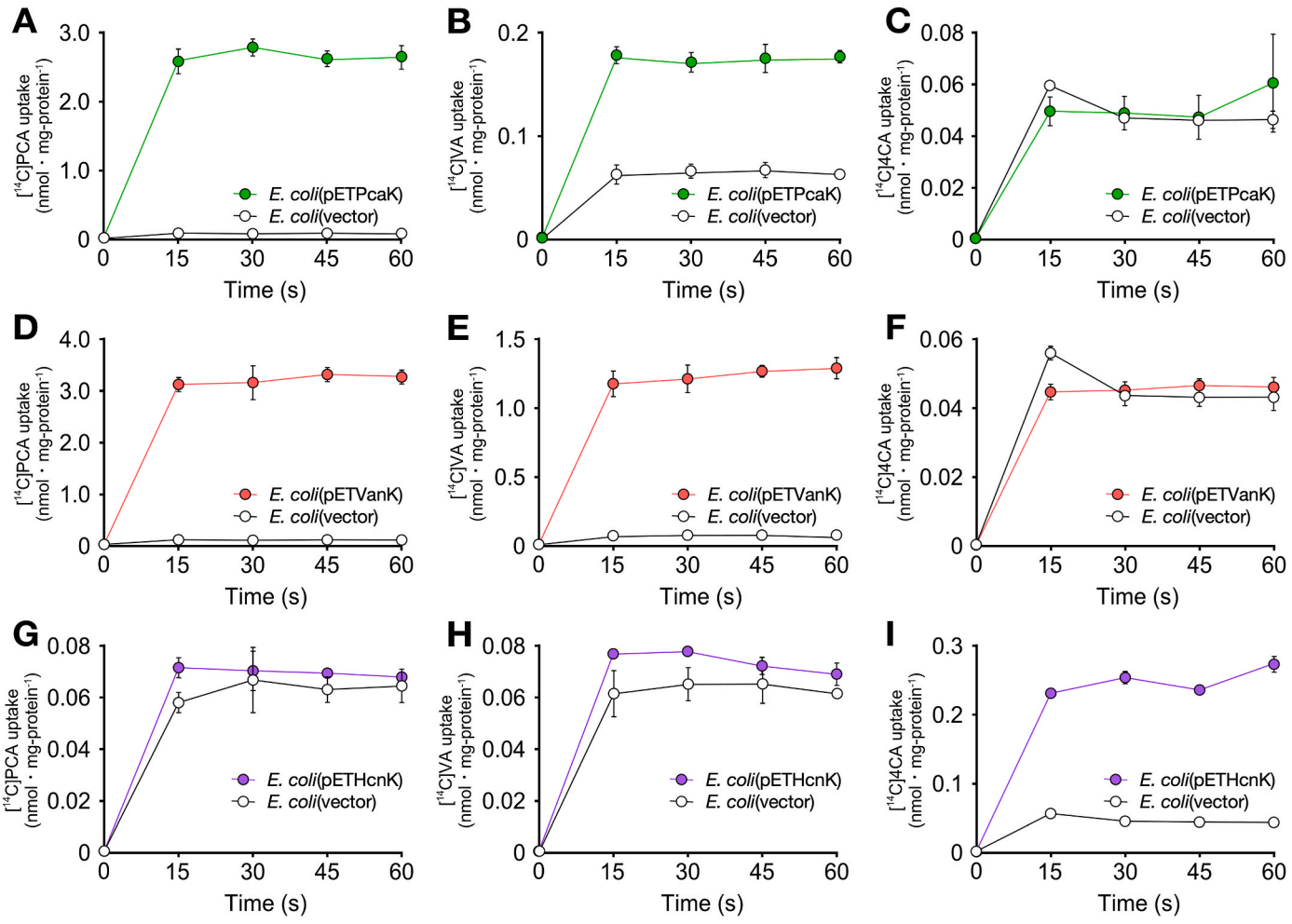

Fig. 6. Uptake of lignin-related monomers by *E. coli* expressing *pcaK*, *vanK*, and *hcnK*. Cells of *E. coli* C43 (DE3) harboring pETPcaK, pETVanK, pETHcnK, or pET-16b (vector) were grown in LB containing IPTG. (**A**–**C**) Cells (OD_{600} = 2.0) of *E. coli* C43 (DE3) (pETPcaK) and *E. coli* C43 (DE3) (pET-16b) were incubated with 20 μM [^{14}C]PCA (**A**), 20 μM [^{14}C]VA (**B**), and 10 μM [^{14}C]4CA (**C**), respectively, in the presence of 10 mM glucose in 50 mM Tris-HCl buffer (pH 7.5). (**D**–**F**) Cells (OD_{600} = 2.0) of *E. coli* C43 (DE3) (pETVanK) and *E. coli* C43 (DE3) (pET-16b) (OD_{600} = 2.0) were incubated with 20 μM [^{14}C]PCA (**D**), 20 μM [^{14}C]VA (**E**), and 10 μM [^{14}C]4CA (**F**), respectively, in the presence of 10 mM glucose in 50 mM Tris-HCl buffer (pH 7.5). (**G**–**I**) Cells (OD_{600} = 2.0) of *E. coli* C43 (DE3) (pETHcnK) and *E. coli* C43 (DE3) (pET-16b) were incubated with 20 μM [^{14}C]PCA (**G**), 20 μM [^{14}C]VA (**H**), and 10 μM [^{14}C]4CA (**I**), respectively, in the presence of 10 mM glucose in 50 mM Tris-HCl buffer (pH 7.5). Portions of the reaction mixtures were collected, and the accumulated radiolabeled substrates inside the cells were measured by liquid scintillation counting. The amount of uptake is expressed as nmol substrate per mg of protein. Each value is the average ± the standard deviation of three independent experiments.

Properties of VanK. Cells of *E. coli* C43 (DE3) harboring a *vanK*-expressing plasmid (pETVanK) showed PCA and VA uptake activities (12.1 ± 0.7 nmol min^{-1} mg^{-1} and 4.4 ± 0.5 nmol min^{-1} mg^{-1}, respectively); however, uptake of 4CA was not observed (Fig. 6D–F). K_m and V_{max} of the uptake of PCA and VA by *E. coli* (pETVanK) cells were estimated to be 12.9 ± 2.7 μM and 28.3 ± 2.4 nmol min^{-1} mg^{-1}, and 8.7 ± 1.6 μM and 5.0 ± 0.3 nmol min^{-1} mg^{-1}, respectively (Supplemental Fig. S9). The uptake rates of VA and PCA by *E. coli* (pETVanK) cells decreased to ca. 4.4% and 2.7% in the presence of 100 μM CCCP compared to the control, indicating that VanK required the proton motive force (Supplemental Fig. S10).

We measured the [^{14}C]PCA and [^{14}C]VA (20 μM) uptake rates by *E. coli* (pETVanK) cells at pH 7.5 in the presence of 20-fold concentration (400 μM) of unlabeled competitor substrates (Supplemental Fig. S11). In the presence of PCA, 4HBA, and VA, the PCA and VA uptake rates reduced to 10% and 17%, 21% and 30%, and 5% and 7%, respectively. These results might suggest that VanK also can uptake 4HBA.

Since V_{max}/K_m of the uptake of PCA by *E. coli* (pETVanK) cells was equivalent to that by *E. coli* (pETPcaK) cells although a direct comparison cannot be made because the expression level is unknown, VanK appeared to be involved in PCA uptake under conditions where *vanK* is induced. It has been reported that the expression of *vanK* was highly induced in KT2440 cells grown on FA or vanillin (D'Arrigo et al., 2019; Simon et al., 2014). When Δ*pcaK* cells grown on VA were used for conversion of PCA, these cells exhibited a higher conversion rate than that by the same cells grown on PCA (Supplemental Fig. S12). Additionally, the conversion rate of PCA by Δ*pcaK vanK* cells grown on VA decreased to the level of Δ*pcaK* cells grown with PCA, once more indicating that *vanK* can participate in the uptake of PCA in an environment where *vanK* is induced.

Properties of HcnK. Cells of *E. coli* C43 (DE3) harboring a *hcnK*-expressing plasmid (pETHcnK) showed a 4CA uptake activity (0.70 ± 0.04 nmol min^{-1} mg^{-1}); however, no apparent uptake of PCA or VA was observed. (Fig. 6G–I). K_m and V_{max} of the 4CA uptake by *E. coli* (pETHcnK) cells were estimated to be 5.2 ± 1.2 μM and 0.7 ± 0.05 nmol min^{-1} mg^{-1}, respectively (Supplemental Fig. S13). The 4CA uptake rate by *E. coli* (pETHcnK) cells decreased to ca. 46% and 30% in the presence of 100 μM and 200 μM CCCP, respectively, compared to the control, suggesting that HcnK required the proton motive force (Supplemental Fig. S14).

To examine the capability of HcnK to uptake FA, we employed a FA/4CA sensor plasmid, pSEVA421-B11 (Siedler et al., 2017). This plasmid carries a *padC* promoter region-YFP gene cassette and *padR*, whose product represses the expression from the *padC* promoter. This repression is released in the presence of FA or 4CA. pSEVA421-B11 and a *hcnK*-expressing plasmid (pSEVAHcnK2) were introduced in *E. coli* XL-2 Blue, and the resulting cells were incubated in Wx medium containing 5 mM glucose with 20 μM FA or 4CA. Fluorescence derived from the expression of the YFP gene was measured at 18 h (Supplemental Fig. S15). The FA uptake activities of *E. coli* cells harboring pSEVA421-B11 grown in the presence and absence of FA were equivalent. The 4CA uptake activity of the same cells was ca. 1.5 times higher in the presence of 4CA than that of the cells grown without FA and CA. When *E. coli* cells harboring both pSEVA421-B11 and pSEVAHcnK2 were incubated with FA and 4CA, the activities were 1.9 times and 3.4 times higher, respectively, than those of the cells grown without FA and 4CA. These results indicate that HcnK functions as a transporter of FA and 4CA.

We measured the [^{14}C]4CA (10 μM) uptake rates by *E. coli* (pETHcnK) cells at pH 7.5 in the presence of 20-fold concentration (200 μM) of unlabeled competitor substrates (Supplemental Fig. S16). The 4CA uptake rates in the presence of C6–C1-type compounds (PCA, 4HBA, VA, syringate, benzoate, 3-hydroxybenzoate, and gallate) were 79–93% of that in the absence of competitive substrates, showing their inhibitory effects were low. On the other hand, in the presence of C6–C3-type compounds, cinnamate and 3-coumarate in addition to 4CA and FA, the 4CA uptake rates decreased to 25–68%. However, no decrease in 4CA uptake was observed in the presence of sinapinate.

3.6. Structural characterization of PcaK, HcnK, VanK, and PP_3658

PcaK, HcnK, VanK, and PP_3658 are expected to share the typical helical fold of MFS transporters, but the significant difference among their sequences (identity between 27 and 34%) presumably confers the variety of substrate specificities described in this study. Aiming to identify the molecular features that likely underlie the different activity properties of these proteins, we predicted their structures and performed comparative analysis centered on key functional regions. For clarity, we focus the structural characterization on PcaK first and then describe the differences and similarities relative to HcnK and VanK.

Ab initio models of the three proteins were generated using evolutionary analysis to infer residue-residue contacts (Hopf et al., 2019). As there are not high-resolution structures of similar homologs currently available to perform homology modeling, our analysis cannot rely on the accuracy of side chain conformations. However, the generated *ab initio* models present good estimated quality (Supplemental Fig. S17), especially in the transmembrane regions, and exhibit the main structural features expected for MFS transporters, indicating that the models are reliable for qualitative structural characterization of these proteins.

The structures of these proteins consist of 12 transmembrane helices (TM), with 1–6 helices and 7–12 helices bundles forming the N-terminal and C-terminal domains, respectively (Fig. 7A). Long peptide segments, rich in positively charged residues, expand toward the cytoplasm. A pair of proton-titratable sites (Asp^{41} and Asp^{44} in PcaK) at TM1 is found in the N-terminal domain cavity. In MFS symporters, these residues are predicted to have lower pK_a than the external pH, avoiding premature protonation (Zhang et al., 2015). Next to these acidic residues, at TM2, there is an arginine (Arg^{124} in PcaK), which is part of a conserved motif (RxxG). Based on previous studies, this positive residue has a role in coupling the substrate-binding pocket with the proton flux at the N-terminal pocket (Fig. 7A and B) (Leano et al., 2019). The location of the substrate-binding site, depicted in Fig. 7, was predicted based on the alignment with *holo* structures of other MFS symporters (PDB id: 6e9o and 1pv7). Upon substrate binding, this arginine is thought to be attracted away from the titratable sites, increasing their pK_a and promoting protonation. In the study of *E. coli* D-galactonate/H$^+$ symporter, substrate translocation is suggested to involve protonation of both titratable residues (Leano et al., 2019). In the mechanism proposed by Jardetzky et al. the protonation triggers the transition between the outward-facing conformation (ground state) and the inward-facing conformation (excited state) of the transporter, which allows the substrate to access the cytoplasm (Jardetzky, 1966).

In addition to the 12-TM fold, these proteins contain other typical structural features of MFS transporters (Fig. 7 and Supplemental

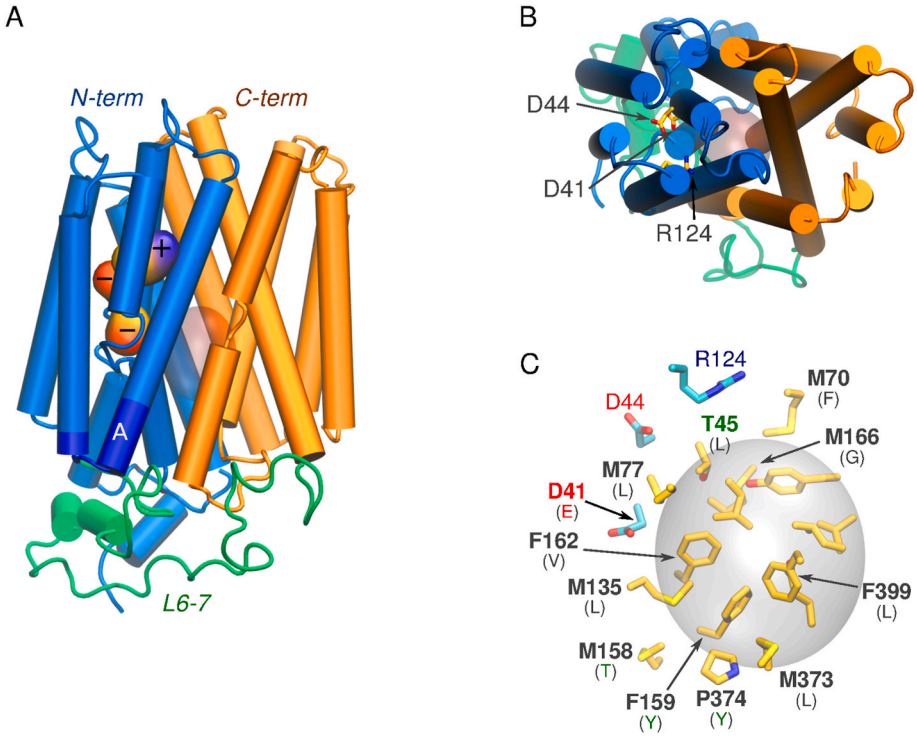

Fig. 7. Structural characterization of PcaK, HcnK and VanK, using the *ab initio* model of PcaK as example. (A) The typical 12-TM helices of MFS transporters. The A-like motif is highlighted in dark blue (labeled with "A"). The two titratable residues, Asp^{41} and Asp^{44}, and Arg^{124} are represented as surfaces in the N-terminal cavity (orange and blue, respectively). The predicted substrate-binding site is indicated with a transparent surface. The interdomain linker (L6-7, in green) is embedded in the cytoplasm. (B) View of the helix bundle from the periplasm. Key residues in the protonation cavity are depicted. (C) Amino acid residues that form the predicted substrate-binding site of PcaK (in yellow). The corresponding residues in HcnK are labeled in parenthesis. Green, red and blue labels indicate polar, acidic and basic amino acids. (For interpretation of the references to colour in this figure legend, the reader is referred to the Web version of this article.)

Fig. S18) (Zhang et al., 2015). An A-like motif (GxxxDRxGRK; residues Gly^{85} to Lys^{94} in PcaK) is found in their cytoplasmic loop L2-3, and it is known to play a critical role in the stabilization of the outward-facing conformation. These proteins also contain a peptide linker, L6-7, connecting the N- and C-terminal domain (Fig. 7 and Supplemental Fig. S18). The dynamics of interactions of positively charged residues and amphipathic regions of L6-7 with the A-like motif and the cell membrane, respectively, are suggested to be involved in the allosteric activation of MFS transporters.

Differences in size and physicochemical properties of the substrate-binding sites among these proteins are likely primary determinants of their uptake activities (Supplemental Table S6). Accordingly, the marked substrate preferences of PcaK and HcnK reflect their very distinct binding sites. In PcaK, we find a greater number of nonpolar and relatively large/long amino acids (i.e., phenylalanines and methionines) in positions corresponding to polar (i.e., tyrosines) and more compact amino acid residues (i.e., leucines and valines) in HcnK (Fig. 7C). The binding site of VanK, in turn, also presents a greater number of hydrophilic sites than PcaK (Supplemental Table S6). Other structural differences are noteworthy. For example, HcnK is the only protein among the putative AAHS family transporters that presents a Glu/Asp titratable pair instead of Asp/Asp and its L6-7 linker is significantly shorter (~28 amino acids) than the corresponding loop in PcaK and VanK (>50 amino acids) (Supplemental Fig. S18).

4. Discussion

Exogenous expression of transporter genes is expected to improve the microbial production of value-added metabolites. For example, Wu et al. reported that introduction of *Rhodopseudomonas palustris* CGA009 *couP*, which encodes a substrate-binding protein of an ABC transporter that has been implicated in the uptake of cinnamate derivatives, into an engineered *E. coli* strain resulted in a 1.3-fold increase in the production of catechol from vanillin (Wu et al., 2018). A 1.24-fold increase in 2-pyrone-4,6-dicarboxylic acid (PDC) production from PCA was achieved when *pcaK* was overexpressed in *Sphingobium* sp. SYK-6 (Mori et al., 2018a). Additionally, the rate of PDC production from 5, 5′-dehydrodivanillate (DDVA) was increased by 1.3-fold by exogenous expression of the inner and outer membrane transporter genes, *ddvK* and *ddvT*, respectively, in the same SYK-6-derived strain (Fujita et al., 2019; Mori et al., 2018b). Towards the goal of the efficient microbial conversion of lignin-related aromatic compounds, here we identified the genes encoding transporters that play a role in the uptake of major lignin-related monomers in *P. putida* KT2440 and described the substrate ranges and uptake kinetics. Taken together, our results increase our collective understanding of the uptake of aromatic acids by *P. putida*.

Δ*pcaK* presented remarkably deficient growth when 2, 5, and 20 mM PCA was used as a carbon and energy source (Fig. 4A) and the PCA conversion rate at pH 7.5 was reduced to ca. 20% of the wild type (Fig. 5A), indicating that PcaK has a major role in PCA uptake. Δ*pcaK* also showed a significant reduction in growth on 2 mM 4HBA, but the difference as compared to wild type diminishes when using higher concentrations of 4HBA (Fig. 4B). The 4HBA conversion rate of Δ*pcaK* (pH 7.5) was reduced to ca. 8% of the wild type (Fig. 5B). Therefore, although PcaK has a major role in 4HBA uptake, the involvement of other transporter(s) with low affinity to 4HBA is suggested. Δ*vanK* showed similar growth as the wild type when 2, 5, and 20 mM of VA was used as a carbon and energy source (Fig. 4C). By contrast, the VA conversion rate of Δ*vanK* (pH 7.5) was reduced to ca. 70% of that of the wild type (Fig. 5C). These results indicate that VanK is involved in VA uptake, in which multiple transporters, including PcaK, seem to participate. Δ*hcnK* was almost entirely deficient in growth on 2 and 5 mM FA, but the growth on 20 mM was comparable to that of the wild type (Fig. 4D). Furthermore, Δ*hcnK* showed a significant decrease in growth on 2 mM 4CA, but the growth on 5 and 20 mM 4CA was comparable to that of the wild type (Fig. 4E). The FA and 4CA conversion rates of Δ*hcnK* (pH 7.5) was reduced to ca. 43% and 23% compared to the wild type (Fig. 5D and E). These results indicate that HcnK has a significant role in FA/4CA uptake; however, additional transporter(s) with low affinity for FA/4CA also appear to be involved in their uptake.

At pH 9.0, the VA conversion rate by Δ*vanK* and the FA/CA conversion rate by Δ*hcnK* were drastically reduced, to ca. 17% and ca. 8% of those by the wild type, respectively (Fig. 5C–E). These results indicate that VanK and HcnK exhibit a major role in the uptake of VA and FA/4CA, respectively, at high pH conditions. Further experiments are needed to explain this pH dependence. Two hypotheses may be considered: 1) the residual passive diffusion of the undissociated form of these aromatic compounds at pH 7.5 is completely abolished at alkaline medium. Similarly, Xu et al. suggested that the complete blockage of passive diffusion may explain the significant decrease in the growth of a transporter-deficient *E. coli* strain at pH 8.2 compared to pH 7.2 on 3-(3-hydroxyphenyl)propionate (pK_a 4.68) (Xu et al., 2013). 2) Background transporters are less active at pH 9.0 due to protein aggregation and/or these transporters are suitable to monoanionic but not dianionic species (carboxylates and phenolates). In addition, the conversion rates of the lignin-related monomers by KT2440 at pH 9.0 were similar to or higher than those at pH 7.0 (these rates are listed in the legend in Fig. 5). This fact suggests that PcaK, VanK, and HcnK have the desirable property of being able to take up the substrates over a wide pH range.

PcaK had a remarkable uptake activity for PCA and also had a slight activity to uptake VA (ca. 5% of activity for PCA uptake) whereas VanK had significant uptake capacity for VA and PCA (Fig. 6A and B). The affinity of VanK for VA (K_m, 8.7 ± 1.6 μM) was slightly higher than that for PCA (K_m, 12.9 ± 2.7 μM), and V_{max} for PCA was about 5.7 times higher than that for VA (supplemental Fig. S9). In addition, the affinity of PcaK for PCA (K_m, 8.1 ± 1.5 μM) was similar to that of VanK (supplemental Fig. S6 and 9A). These K_m values are close to those of *P. putida* PRS2000 PcaK (6 μM) for 4HBA and of *P. putida* KTGAL GalT for PCA (9.1 μM) (Nichols and Harwood, 1997; Nogales et al., 2011). HcnK had the ability to take up 4CA, and its K_m for 4CA was estimated to be 5.2 ± 1.2 μM (Fig. 6I; supplemental Fig. S13). Additionally, the bioassay showed that HcnK also could take up FA (Supplemental Fig. S15). From the substrate competition experiments, the uptake of 4CA by HcnK was strongly inhibited in the presence of C6–C3 compounds such as 4CA, FA, cinnamate, and 3-coumarate, and was also inhibited in the presence of caffeate and 3-methoxycinnamate (Supplemental Fig. S16). On the other hand, slight inhibition was observed in the presence of the C6–C1 compounds, 4HBA and VA. These results suggest that HcnK is selective to C6–C3 compounds. Among C6–C3 compounds tested, sinapinate showed no inhibition on the uptake of 4CA by HcnK, suggesting that the presence of methoxy groups at both C3 and C5 positions is inhibitory for HcnK substrate recognition.

Finally, structural analyses indicate that the size and the hydropathic properties of the substrate binding sites of PcaK, HcnK, and VanK likely impact their substrate preferences. The tighter substrate pocket of PcaK may explain the transport activity for smaller substrates such as PCA and 4HBA, as compared to the larger HcnK substrates, FA/4CA (Fig. 7). The predominantly hydrophobic pocket of PcaK is somewhat surprising as its major substrates are relatively more hydrophilic. However, an abundance of polar residues and hydrogen bond-interacting sites would lead to higher binding affinity and, thus, impair the rapid flux of the substrate. Conversely, the wider binding site of HcnK and the presence of hydrophilic residues (Tyr^{142} and Tyr^{326}) is compatible with its more efficient transport activity for relatively large, hydrophobic substrates. Similarly, based on the hypothesis of substrate flux optimization, the fact that the binding site of VanK contains more hydrophilic sites than PcaK, is consistent with its preference for a more hydrophobic substrate (i.e., VA compared to PCA).

Notably, despite their low global identity (26%), the composition of the actual binding site of PP_3658 is very similar to that of HcnK (72%) (Supplemental Table S6). The most relevant differences between the substrate pockets of these proteins are the amino acid residues Phe^{151}/

Tyr^{142}, Tyr^{154}/Val^{145}, and Thr^{69}/Leu^{60}, in PP_3658 and HcnK, respectively. It is possible that PP_3658 does not exhibit a prominent uptake activity towards FA ad 4CA, like HcnK does, due to the steric hindrance of the cavity entrance by the bulky Tyr^{154}. Other structural differences may indirectly contribute to the specificity of these transporters. HcnK, on the other hand, contains the unique heterogeneous pair of titratable residues, Glu^{24}/Asp^{27}. The substitution of the titratable glutamate by aspartate in the *E. coli* 3-(3-hydroxy-phenyl)propionate) transporter (56% identical to HcnK) results in a slight decrease in transport activity (Xu et al., 2013). It appears that the higher pK_a of Glu (2.2) compared to Asp (1.9) represents a lower energy barrier for protonation upon substrate binding (Lide, 1991). Additionally, the considerably shorter interdomain linker of HcnK may be important. Zhang et al. suggest that this linker is stretched in the inward-facing conformation of MFS transporters, forming critical contacts for the stabilization of this state (Zhang et al., 2015). Inferring how these two features possibly affect transport activity is not straightforward and should be the subject of future studies.

5. Conclusions

We found that members of the AAHS family transporters, PcaK and HcnK, play a significant role in the uptake of PCA/4HBA and FA/4CA in *P. putida* KT2440, and VanK is involved in the VA uptake. In addition, comparative structural analyses suggest the key molecular features underlying the distinct activity profiles of these transporters. Taken together, these findings are expected to contribute to improving the efficiency of conversion of lignin-related monomers into valuable chemicals by optimizing the uptake capacity of *P. putida* KT2440, providing similar capacity to other host strains, and modulating the substrate preferences of the individual transporters through protein engineering.

CRediT authorship contribution statement

Ayumu Wada: Investigation, Writing - original draft. **Érica T. Prates:** Investigation, Writing - original draft, Writing - Review & Editing. **Ryo Hirano:** Investigation. **Allison Z. Werner:** Writing - Review & Editing. **Naofumi Kamimura:** Supervision, Formal analysis, Writing - original draft, Writing - Review & Editing. **Daniel A. Jacobson:** Supervision, Funding acquisition, Writing - Review & Editing. **Gregg T. Beckham:** Conceptualization, Supervision, Funding acquisition, Writing - Review & Editing. **Eiji Masai:** Conceptualization, Supervision, Funding acquisition, Writing - original draft, Writing - Review & Editing.

Acknowledgements

We thank Drs. Esteban Martínez and Victor de Lorenzo for providing the pEMG/pSW-2 system. We also thank Dr. Morten Sommer for providing pSEVA421-B11. This work was supported in part by JSPS KAKENHI (19H02867), Japan. E.T.P, A.Z.W, D.A.J, and G.T.B acknowledge funding from the Center for Bioenergy Innovation, a U.S. Department of Energy Bioenergy Research Center supported by the Office of Biological and Environmental Research in the DOE Office of Science, United States. This manuscript has been partially authored by UT-Battelle, LLC under Contract No. DE-AC05-00OR22725 with the U.S. Department of Energy. Additionally, this work was authored in part by the Alliance for Sustainable Energy, LLC, the manager and operator of the National Renewable Energy Laboratory for the U.S. Department of Energy under Contract No. DE-AC36-08GO28308. The views expressed in the article do not necessarily represent the views of the DOE or the U. S. Government. The U.S. Government retains and the publisher, by accepting the article for publication, acknowledges that the U.S. Government retains a nonexclusive, paid-up, irrevocable, worldwide license to publish or reproduce the published form of this work, or allow others to do so, for U.S. Government purposes.

Appendix A. Supplementary data

Supplementary data to this article can be found online at https://doi.org/10.1016/j.ymben.2021.01.013.

References

Araki, T., Tanatani, K., Kamimura, N., Otsuka, Y., Yamaguchi, M., Nakamura, M., Masai, E., 2020. The syringate *O*-demethylase gene of *Sphingobium* sp. strain SYK-6 is regulated by DesX, while other vanillate and syringate catabolism genes are regulated by DesR. Appl. Environ. Microbiol. 86, e01712-20.

Becker, J., Wittmann, C., 2019. A field of dreams: lignin valorization into chemicals, materials, fuels, and health-care products. Biotechnol. Adv. 37, 107360.

Beckham, G.T., Johnson, C.W., Karp, E.M., Salvachúa, D., Vardon, D.R., 2016. Opportunities and challenges in biological lignin valorization. Curr. Opin. Biotechnol. 42, 40–53.

Beltrán, J.L., Sanli, N., Fonrodona, G., Barrón, D., Özkan, G., Barbosa, J., 2003. Spectrophotometric, potentiometric and chromatographic p*K*a values of polyphenolic acids in water and acetonitrile–water media. Anal. Chim. Acta 484, 253–264.

Bugg, T.D., Ahmad, M., Hardiman, E.M., Rahmanpour, R., 2011. Pathways for degradation of lignin in bacteria and fungi. Nat. Prod. Rep. 28, 1883–1896.

Chaudhry, M.T., Huang, Y., Shen, X.H., Poetsch, A., Jiang, C.Y., Liu, S.J., 2007. Genome-wide investigation of aromatic acid transporters in *Corynebacterium glutamicum*. Microbiology 153, 857–865.

Chen, Z., Huang, J., Wu, Y., Wu, W., Zhang, Y., Liu, D., 2017. Metabolic engineering of *Corynebacterium glutamicum* for the production of 3-hydroxypropionic acid from glucose and xylose. Metab. Eng. 39, 151–158.

Collier, L.S., Nichols, N.N., Neidle, E.L., 1997. *benK* encodes a hydrophobic permease-like protein involved in benzoate degradation by *Acinetobacter* sp. strain ADP1. J. Bacteriol. 179, 5943–5946.

D'Arrigo, I., Cardoso, J.G.R., Rennig, M., Sonnenschein, N., Herrgard, M.J., Long, K.S., 2019. Analysis of *Pseudomonas putida* growth on non-trivial carbon sources using transcriptomics and genome-scale modelling. Environ Microbiol Rep 11, 87–97.

D'Argenio, D.A., Segura, A., Coco, W.M., Bünz, P.V., Ornston, L.N., 1999. The physiological contribution of *Acinetobacter* PcaK, a transport system that acts upon protocatechuate, can be masked by the overlapping specificity of VanK. J. Bacteriol. 181, 3505–3515.

Frank, A.M., Chua, M.J., Gulvik, C.A., Buchan, A., 2018. Functional redundancy in the hydroxycinnamate catabolism pathways of the salt marsh bacterium *Sagittula stellata* E-37. Appl. Environ. Microbiol. 84, e02027-18.

Fujita, M., Mori, K., Hara, H., Hishiyama, S., Kamimura, N., Masai, E., 2019. A TonB-dependent receptor constitutes the outer membrane transport system for a lignin-derived aromatic compound. Commun Biol 2, 432.

Harwood, C.S., Nichols, N.N., Kim, M.K., Ditty, J.L., Parales, R.E., 1994. Identification of the *pcaRKF* gene cluster from *Pseudomonas putida*: involvement in chemotaxis, biodegradation, and transport of 4-hydroxybenzoate. J. Bacteriol. 176, 6479–6488.

Hopf, T.A., Colwell, L.J., Sheridan, R., Rost, B., Sander, C., Marks, D.S., 2012. Three-dimensional structures of membrane proteins from genomic sequencing. Cell 149, 1607–1621.

Hopf, T.A., Green, A.G., Schubert, B., Mersmann, S., Scharfe, C.P.I., Ingraham, J.B., Toth-Petroczy, A., Brock, K., Riesselman, A.J., Palmedo, P., Kang, C., Sheridan, R., Draizen, E.J., Dallago, C., Sander, C., Marks, D.S., 2019. The EVcouplings Python framework for coevolutionary sequence analysis. Bioinformatics 35, 1582–1584.

Humphrey, W., Dalke, A., Schulten, K., 1996. VMD: visual molecular dynamics. J. Mol. Graph. 14, 33–38.

Incha, M.R., Thompson, M.G., Blake-Hedges, J.M., Liu, Y., Pearson, A.N., Schmidt, M., Gin, J.W., Petzold, C.J., Deutschbauer, A.M., Keasling, J.D., 2020. Leveraging host metabolism for bisdemethoxycurcumin production in *Pseudomonas putida*. Metab Eng Commun 10, e00119.

Jardetzky, O., 1966. Simple allosteric model for membrane pumps. Nature 211, 969–970.

Jiménez, J.I., Miñambres, B., García, J.L., Díaz, E., 2002. Genomic analysis of the aromatic catabolic pathways from *Pseudomonas putida* KT2440. Environ. Microbiol. 4, 824–841.

Johnson, C.W., Abraham, P.E., Linger, J.G., Khanna, P., Hettich, R.L., Beckham, G.T., 2017. Eliminating a global regulator of carbon catabolite repression enhances the conversion of aromatic lignin monomers to muconate in *Pseudomonas putida* KT2440. Metab Eng Commun 5, 19–25.

Johnson, C.W., Salvachúa, D., Rorrer, N.A., Black, B.A., Vardon, D.R., St John, P.C., Cleveland, N.S., Dominick, G., Elmore, J.R., Grundl, N., Khanna, P., Martinez, C.R., Michener, W.E., Peterson, D.J., Ramirez, K.J., Singh, P., VanderWall, T.A., Wilson, A. N., Yi, X.N., Biddy, M.J., Bomble, Y.J., Guss, A.M., Beckham, G.T., 2019. Innovative chemicals and materials from bacterial aromatic catabolic pathways. Joule 3, 1523–1537.

Kallscheuer, N., Vogt, M., Kappelmann, J., Krumbach, K., Noack, S., Bott, M., Marienhagen, J., 2016. Identification of the *phd* gene cluster responsible for phenylpropanoid utilization in *Corynebacterium glutamicum*. Appl. Microbiol. Biotechnol. 100, 1871–1881.

Kamimura, N., Aoyama, T., Yoshida, R., Takahashi, K., Kasai, D., Abe, T., Mase, K., Katayama, Y., Fukuda, M., Masai, E., 2010. Characterization of the protocatechuate

4,5-cleavage pathway operon in *Comamonas* sp. strain E6 and discovery of a novel pathway gene. Appl. Environ. Microbiol. 76, 8093–8101.
Kamimura, N., Takahashi, K., Mori, K., Araki, T., Fujita, M., Higuchi, Y., Masai, E., 2017. Bacterial catabolism of lignin-derived aromatics: new findings in a recent decade: update on bacterial lignin catabolism. Environ Microbiol Rep 9, 679–705.
Koehler Leman, J., Ulmschneider, M.B., Gray, J.J., 2015. Computational modeling of membrane proteins. Proteins 83, 1–24.
Larkin, M.A., Blackshields, G., Brown, N.P., Chenna, R., McGettigan, P.A., McWilliam, H., Valentin, F., Wallace, I.M., Wilm, A., Lopez, R., Thompson, J.D., Gibson, T.J., Higgins, D.G., 2007. Clustal W and clustal X version 2.0. Bioinformatics 23, 2947–2948.
Leano, J.B., Batarni, S., Eriksen, J., Juge, N., Pak, J.E., Kimura-Someya, T., Robles-Colmenares, Y., Moriyama, Y., Stroud, R.M., Edwards, R.H., 2019. Structures suggest a mechanism for energy coupling by a family of organic anion transporters. PLoS Biol. 17, e3000260.
Lide, D.R., 1991. Handbook of Chemistry and Physics. CRC Press, Boca Raton, FL.
Linger, J.G., Vardon, D.R., Guarnieri, M.T., Karp, E.M., Hunsinger, G.B., Franden, M.A., Johnson, C.W., Chupka, G., Strathmann, T.J., Pienkos, P.T., Beckham, G.T., 2014. Lignin valorization through integrated biological funneling and chemical catalysis. Proc. Natl. Acad. Sci. U. S. A. 111, 12013–12018.
Loeschcke, A., Thies, S., 2015. *Pseudomonas putida*-a versatile host for the production of natural products. Appl. Microbiol. Biotechnol. 99, 6197–6214.
MacLean, A.M., Haerty, W., Golding, G.B., Finan, T.M., 2011. The LysR-type PcaQ protein regulates expression of a protocatechuate-inducible ABC-type transport system in *Sinorhizobium meliloti*. Microbiology 157, 2522–2533.
Madeira, F., Park, Y.M., Lee, J., Buso, N., Gur, T., Madhusoodanan, N., Basutkar, P., Tivey, A.R.N., Potter, S.C., Finn, R.D., Lopez, R., 2019. The EMBL-EBI search and sequence analysis tools APIs in 2019. Nucleic Acids Res. 47, W636–W641.
Martinez-Garcia, E., de Lorenzo, V., 2011. Engineering multiple genomic deletions in Gram-negative bacteria: analysis of the multi-resistant antibiotic profile of *Pseudomonas putida* KT2440. Environ. Microbiol. 13, 2702–2716.
Masai, E., Katayama, Y., Fukuda, M., 2007. Genetic and biochemical investigations on bacterial catabolic pathways for lignin-derived aromatic compounds. Biosci. Biotechnol. Biochem. 71, 1–15.
Michalska, K., Chang, C., Mack, J.C., Zerbs, S., Joachimiak, A., Collart, F.R., 2012. Characterization of transport proteins for aromatic compounds derived from lignin: benzoate derivative binding proteins. J. Mol. Biol. 423, 555–575.
Mohamed, E.T., Werner, A.Z., Salvachúa, D., Singer, C.A., Szostkiewicz, K., Rafael Jiménez-Díaz, M., Eng, T., Radi, M.S., Simmons, B.A., Mukhopadhyay, A., Herrgård, M.J., Singer, S.W., Beckham, G.T., Feist, A.M., 2020. Adaptive laboratory evolution of *Pseudomonas putida* KT2440 improves *p*-coumaric and ferulic acid catabolism and tolerance. Metab Eng Commun 11, e00143.
Mori, K., Kamimura, N., Masai, E., 2018a. Identification of the protocatechuate transporter gene in *Sphingobium* sp. strain SYK-6 and effects of overexpression on production of a value-added metabolite. Appl. Microbiol. Biotechnol. 102, 4807–4816.
Mori, K., Niinuma, K., Fujita, M., Kamimura, N., Masai, E., 2018b. DdvK, a novel major facilitator superfamily transporter essential for 5,5'-dehydrodivanillate uptake by *Sphingobium* sp. strain SYK-6. Appl. Environ. Microbiol. 84, e01314-18.
Nichols, N.N., Harwood, C.S., 1997. PcaK, a high-affinity permease for the aromatic compounds 4-hydroxybenzoate and protocatechuate from *Pseudomonas putida*. J. Bacteriol. 179, 5056–5061.
Nikel, P.I., Chavarria, M., Danchin, A., de Lorenzo, V., 2016. From dirt to industrial applications: *Pseudomonas putida* as a synthetic biology chassis for hosting harsh biochemical reactions. Curr. Opin. Chem. Biol. 34, 20–29.
Nishikawa, Y., Yasumi, Y., Noguchi, S., Sakamoto, H., Nikawa, J., 2008. Functional analyses of *Pseudomonas putida* benzoate transporters expressed in the yeast *Saccharomyces cerevisiae*. Biosci. Biotechnol. Biochem. 72, 2034–2038.
Nogales, J., Canales, Á., Jiménez-Barbero, J., Serra, B., Pingarrón, J.M., García, J.L., Díaz, E., 2011. Unravelling the gallic acid degradation pathway in bacteria: the *gal* cluster from *Pseudomonas putida*. Mol. Microbiol. 79, 359–374.
Otani, H., Lee, Y.E., Casabon, I., Eltis, L.D., 2014. Characterization of *p*-hydroxycinnamate catabolism in a soil Actinobacterium. J. Bacteriol. 196, 4293–4303.
Pao, S.S., Paulsen, I.T., Saier, M.H., 1998. Major facilitator superfamily. Microbiol. Mol. Biol. Rev. 62, 1–34.
Pernstich, C., Senior, L., MacInnes, K.A., Forsaith, M., Curnow, P., 2014. Expression, purification and reconstitution of the 4-hydroxybenzoate transporter PcaK from *Acinetobacter* sp. ADP1. Protein Expr Purif 101, 68–75.
Poblete-Castro, I., Becker, J., Dohnt, K., dos Santos, V.M., Wittmann, C., 2012. Industrial biotechnology of *Pseudomonas putida* and related species. Appl. Microbiol. Biotechnol. 93, 2279–2290.
Ragauskas, A.J., Beckham, G.T., Biddy, M.J., Chandra, R., Chen, F., Davis, M.F., Davison, B.H., Dixon, R.A., Gilna, P., Keller, M., Langan, P., Naskar, A.K., Saddler, J. N., Tschaplinski, T.J., Tuskan, G.A., Wyman, C.E., 2014. Lignin valorization: improving lignin processing in the biorefinery. Science 344, 1246843.
Ravi, K., Garcia-Hidalgo, J., Gorwa-Grauslund, M.F., Liden, G., 2017. Conversion of lignin model compounds by *Pseudomonas putida* KT2440 and isolates from compost. Appl. Microbiol. Biotechnol. 101, 5059–5070.
Reddy, V.S., Shlykov, M.A., Castillo, R., Sun, E.I., Saier Jr., M.H., 2012. The major facilitator superfamily (MFS) revisited. FEBS J. 279, 2022–2035.
Reveron, I., Jimenez, N., Curiel, J.A., Penas, E., Lopez de Felipe, F., de Las Rivas, B., Munoz, R., 2017. Differential gene expression by *Lactobacillus plantarum* WCFS1 in response to phenolic compounds reveals new genes involved in tannin degradation. Appl. Environ. Microbiol. 83, e03387-16.
Saier Jr., M.H., Reddy, V.S., Tsu, B.V., Ahmed, M.S., Li, C., Moreno-Hagelsieb, G., 2016. The transporter classification database (TCDB): recent advances. Nucleic Acids Res. 44, D372–D379.
Salmon, R.C., Cliff, M.J., Rafferty, J.B., Kelly, D.J., 2013. The CouPSTU and TarPQM transporters in *Rhodopseudomonas palustris*: redundant, promiscuous uptake systems for lignin-derived aromatic substrates. PloS One 8, e59844.
Salvachúa, D., Johnson, C.W., Singer, C.A., Rohrer, H., Peterson, D.J., Black, B.A., Knapp, A., Beckham, G.T., 2018. Bioprocess development for muconic acid production from aromatic compounds and lignin. Green Chem. 20, 5007–5019.
Salvachúa, D., Rydzak, T., Auwae, R., De Capite, A., Black, B.A., Bouvier, J.T., Cleveland, N.S., Elmore, J.R., Huenemann, J.D., Katahira, R., Michener, W.E., Peterson, D.J., Rohrer, H., Vardon, D.R., Beckham, G.T., Guss, A.M., 2020. Metabolic engineering of *Pseudomonas putida* for increased polyhydroxyalkanoate production from lignin. Microb Biotechnol 13, 290–298.
Siedler, S., Khatri, N.K., Zsohár, A., Kjærbølling, I., Vogt, M., Hammar, P., Nielsen, C.F., Marienhagen, J., Sommer, M.O.A., Joensson, H.N., 2017. Development of a bacterial biosensor for rapid screening of yeast *p*-coumaric acid production. ACS Synth. Biol. 6, 1860–1869.
Simon, O., Klaiber, I., Huber, A., Pfannstiel, J., 2014. Comprehensive proteome analysis of the response of *Pseudomonas putida* KT2440 to the flavor compound vanillin. J Proteomics 109, 212–227.
Sonoki, T., Takahashi, K., Sugita, H., Hatamura, M., Azuma, Y., Sato, T., Suzuki, S., Kamimura, N., Masai, E., 2017. Glucose-free *cis,cis*-muconic acid production via new metabolic designs corresponding to the heterogeneity of lignin. ACS Sustain. Chem. Eng. 6, 1256–1264.
Studer, G., Biasini, M., Schwede, T., 2014. Assessing the local structural quality of transmembrane protein models using statistical potentials (QMEANBrane). Bioinformatics 30, i505–511.
Suzuki, Y., Okamura-Abe, Y., Nakamura, M., Otsuka, Y., Araki, T., Otsuka, H., Navarro, R.R., Kamimura, N., Masai, E., Katayama, Y., 2020. Development of the production of 2-pyrone-4,6-dicarboxylic acid from lignin extracts, which are industrially formed as by-products, as raw materials. J. Biosci. Bioeng. 130, 71–75.
Vermaas, J.V., Dixon, R.A., Chen, F., Mansfield, S.D., Boerjan, W., Ralph, J., Crowley, M. F., Beckham, G.T., 2019. Passive membrane transport of lignin-related compounds. Proc. Natl. Acad. Sci. U. S. A. 116, 23117–23123.
Weimer, A., Kohlstedt, M., Volke, D.C., Nikel, P.I., Wittmann, C., 2020. Industrial biotechnology of *Pseudomonas putida*: advances and prospects. Appl. Microbiol. Biotechnol. 104, 7745–7766.
Wu, W., Liu, F., Singh, S., 2018. Toward engineering *E. coli* with an autoregulatory system for lignin valorization. Proc. Natl. Acad. Sci. U. S. A. 115, 2970–2975.
Xu, Y., Chen, B., Chao, H., Zhou, N.Y., 2013. *mhpT* encodes an active transporter involved in 3-(3-hydroxyphenyl)propionate catabolism by *Escherichia coli* K-12. Appl. Environ. Microbiol. 79, 6362–6368.
Xu, Y., Wang, S.H., Chao, H.J., Liu, S.J., Zhou, N.Y., 2012. Biochemical and molecular characterization of the gentisate transporter GenK in *Corynebacterium glutamicum*. PloS One 7, e38701.
Zhang, X.C., Zhao, Y., Heng, J., Jiang, D., 2015. Energy coupling mechanisms of MFS transporters. Protein Sci. 24, 1560–1579.